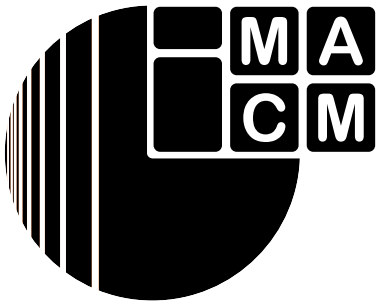

Bergische Universität Wuppertal

Fachbereich Mathematik und Naturwissenschaften

Institute of Mathematical Modelling, Analysis and Computational Mathematics (IMACM)

Preprint BUW-IMACM 15/31

Kai Gausling, Andreas Bartel

Coupling Interfaces and their Impact in Field/Circuit Co-Simulation

July 29, 2015

http://www.math.uni-wuppertal.de

Coupling Interfaces and their Impact in Field/Circuit Co-Simulation

Kai Gausling, Andreas Bartel

Chair of Applied Mathematics / Numerical Analysis, Bergische Universität Wuppertal, 42119 Wuppertal, Germany

For the time domain simulation of coupled systems, co-simulation is a prominent approach. The contraction and the speed of convergence of corresponding schemes depend on the design of the coupling interface and the computational order amongst others. Here the field/circuit coupling is investigated, where the standard approach of decoupling is to separate between the field and circuit part. In this context we introduce a new decoupling approach: LR-coupling. For this coupling type, general stability and contraction follow directly from the coupling interface. Thus these properties are independent from embedded electric networks or embedded EM devices. Furthermore, first investigations demonstrate that using a dedicated coupling interface may enhance the convergence properties, i.e., it may reduce the computational effort for prescribed tolerances.

***Index Terms*—Circuit simulation, Coupling circuits, Circuit subsystems, Electromagnetic devices, Stability criteria, Convergence**

I. Introduction

Coupling of software tools is a standard technique for simulation of coupled multiphysics problems. Each simulator is used to compute the solution of its own subproblem. Thus information between these subproblems have to be exchanged. To enhance convergence, this process works on certain time periods (windows), where convergence can be achieved by solving multiple times the subsystems. This procedure is called co-simulation, dynamic iteration or waveform relaxation. Our focus is on time integration of field/circuit coupled problems, which yields coupled systems of differential algebraic equations (DAEs). Co-simulation applied to coupled ordinary differential equations (ODEs) always convergences, see e.g. [3]. However, dynamic iteration of DAE might fail, if certain contraction condition is not fulfilled, see e.g. [1]. Here we aim to design a coupling interface, which ensures convergency for any system of coupled DAEs (only constraint: DAE-index≤ 1).

The paper is organized as follows: Sec. 2 summarizes circuit and field models and introduces the notation of coupled problems. Sec. 3 gives inside into the well known co-simulation procedure. As alternative to the cutting at EM device boundaries, a new approach of coupling is proposed and analyzed in Sec. 4, which we termed the LR-coupling. In Sec. 5 our test problem is presented with a theoretical convergence analysis for both (de-)coupling approaches. Sec. 6 proves the theoretical results numerically and discusses the results.

II. Modeling

An electric circuit can be described by modified nodal analysis (MNA). The corresponding mathematical model reads:

$$\begin{aligned} \boldsymbol{A}_C \frac{d}{dt}\boldsymbol{q}(\boldsymbol{A}_C^T\boldsymbol{u}) + \boldsymbol{A}_R\boldsymbol{g}_R(\boldsymbol{A}_R^T\boldsymbol{u}) \\ +\boldsymbol{A}_L\boldsymbol{i}_L + \boldsymbol{A}_V\boldsymbol{i}_V + \boldsymbol{A}_I\boldsymbol{i}_S(t) + \boldsymbol{A}_M\boldsymbol{i}_M = 0, \\ \frac{d}{dt}\Phi(\boldsymbol{i}_L) - \boldsymbol{A}_L^T\boldsymbol{u} = 0, \\ \boldsymbol{A}_V^T\boldsymbol{u} - \boldsymbol{v}_S(t) = 0 \end{aligned}$$

with incidence matrices $\boldsymbol{A}_\star$ (for the topology), charges $\boldsymbol{q}$, fluxes Φ, conductances $\boldsymbol{g}_R$ and with the unknown node potentials $\boldsymbol{u}$, and unknown currents through inductors $\boldsymbol{i}_L$ and voltage sources $\boldsymbol{i}_V$. Independent sources are $\boldsymbol{i}_S, \boldsymbol{v}_S$. Furthermore $\boldsymbol{i}_M$ denotes a coupling current (current through MQS-devise). Furthermore, the magnetic field of any MQS-device can be described by the spatially discretized curl-curl equations terms of the discretized magnetic vector potential $\boldsymbol{a}$:

$$\boldsymbol{M}_\sigma \frac{d}{dt}\boldsymbol{a} + \boldsymbol{k}_\nu(\boldsymbol{a})\boldsymbol{a} - \boldsymbol{X}_M\boldsymbol{i}_M = 0$$

using the conductivity $\boldsymbol{M}_\sigma$, the nonlinear curl-curl matrix $\boldsymbol{k}_\nu$ and a distribution matrix $\boldsymbol{X}_M$ for the corresponding currents $\boldsymbol{i}_M$ [6]. Finally, each MQS-device has a system of coupling equations [5]: (using resistivity of the MQS-device $\boldsymbol{R}_M$)

$$\boldsymbol{X}_M^T \frac{d}{dt}\boldsymbol{a} + \boldsymbol{R}_M\boldsymbol{i}_M - \boldsymbol{A}_M^T\boldsymbol{u} = 0.$$

For an index-1 network, the whole system (field/circuit) can be described as differential algebraic initial-value problem

$$\begin{aligned} \dot{\boldsymbol{y}} &= \boldsymbol{f}(t, \boldsymbol{y}, \boldsymbol{z}) \qquad \text{with } \boldsymbol{y}(t_0) = \boldsymbol{y_0} \\ \boldsymbol{0} &= \boldsymbol{g}(t, \boldsymbol{y}, \boldsymbol{z}, \boldsymbol{x}) \end{aligned} \tag{1}$$

with differential $\boldsymbol{y} := (\boldsymbol{q}, \boldsymbol{\Phi}, \boldsymbol{a})^\top$ and algebraic unknown $\boldsymbol{z} := (\boldsymbol{u}, \boldsymbol{i}_l, \boldsymbol{i}_V)^\top$. System (1) is referred to as strongly coupled.

III. Co-simulation Fundamentals

Usually, the simulation time $[T_0, T_{\text{end}}]$ is split into time windows $[T_n, T_{n+1}]$ with $0 = T_0 < T_1 < \cdots < T_N = T_{\text{end}}$. Then co-simulation operates on these time windows with communication step size $H_n := T_{n+1} - T_n$. The Gauss-Seidel approach computes the solution of the coupled problem sequentially and iteratively: each subproblem is solved with coupling terms fixed to the (best) so far known approximation. Thereby each subsystem may employ a dedicated time integrator (with dedicated step sizes h). To start co-simulation, one has to select, which subsystem is computed first. Any co-simulation model is referred to as weakly coupled.

For system (1), any co-simulation procedure can be encode by splitting functions $\boldsymbol{F}, \boldsymbol{G}$:

$$\begin{aligned} \dot{\boldsymbol{y}} = \boldsymbol{f}(\boldsymbol{y}, \boldsymbol{z}) \leftrightarrow\ \dot{\tilde{\boldsymbol{y}}}^{(k)} &= \boldsymbol{F}\Big(\tilde{\boldsymbol{y}}^{(k)}, \tilde{\boldsymbol{z}}^{(k)}, \tilde{\boldsymbol{y}}^{(k-1)}, \tilde{\boldsymbol{z}}^{(k-1)}\Big) \\ \boldsymbol{0} = \boldsymbol{g}(\boldsymbol{y}, \boldsymbol{z}) \qquad \boldsymbol{0} &= \boldsymbol{G}\Big(\tilde{\boldsymbol{y}}^{(k)}, \tilde{\boldsymbol{z}}^{(k)}, \tilde{\boldsymbol{y}}^{(k-1)}, \tilde{\boldsymbol{z}}^{(k-1)}\Big), \end{aligned} \tag{2}$$

where the superscript (k) and $(k-1)$ address the current and old iterates. $\boldsymbol{F}$, $\boldsymbol{G}$ have to fulfill compartibility [1]. For simplicity, we drop the tilde in the following.

Starting from two solutions on the nth time window $[T_n, T_{n+1}]$ and performing k iterations of the co-simulation scheme, the accuracy of the solution is measured from the differences $\delta^{(k)}_{\boldsymbol{y},n} := \sup_{t\in[T_n,T_{n+1}]} \|\boldsymbol{y}^{(k)}_n(t) - \tilde{\boldsymbol{y}}^{(k)}_n(t)\|_2$ (etc.).

For (2), one can derive the following recursion estimate:

$$\begin{pmatrix}\delta^{(k)}_{y,n}\\ \delta^{(k)}_{z,n}\end{pmatrix} \le \begin{pmatrix} CH_n & CH_n \\ C & CH_n+\alpha_n\end{pmatrix}\begin{pmatrix}\delta^{(k-1)}_{y,n}\\ \delta^{(k-1)}_{z,n}\end{pmatrix} + \text{"initial offset"},$$

with differential and algebraic splitting error $\delta^{(k)}_{y,n}$ and $\delta^{(k)}_{z,n}$, constant $C>0$ and contraction factor α_n, see, e.g., [4]. If $0<\alpha_n<1$, one observes the constant contraction rate α_n. If $\alpha_n = 0$ higher rates can be obtained, see [4].

We compare two different decoupling approaches: a) cutting at the EM device boundary (classical approach) [5]. b) the proposed LR-coupling technique, see below. Furthermore, we employ here source coupling, where the data exchange is facilitated via controlled sources. In fact there exist more advanced techniques, see, e.g., [2].

IV. LR-Coupling Interface and Analysis

We expand the coupling interface by introducing or identifying an LR-link, which may model some physical wire in the respective location. Using decoupling with controlled sources, this situation is sketched in Fig. 1, where NW 1 and NW 2 signify each an arbitrary network (circuit or EM device).

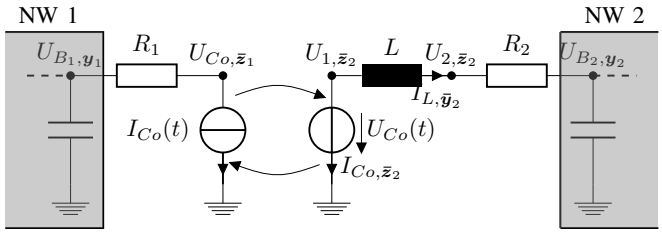

Fig. 1. Decoupling via sources and using an LR-interface. The bar-notation is used to refer explicitly to the type of unknowns in the LR-coupling.

For a Gauß-Seidel type scheme, the splitting functions read: here $\boldsymbol{y}_i$, $\boldsymbol{z}_i$ represent the unknowns NW i

$$\begin{bmatrix}\dot{\boldsymbol{y}}_1^{(k)}\\ \hline \dot{\boldsymbol{y}}_2^{(k)}\end{bmatrix} = \boldsymbol{F} := \left[\begin{array}{l} \boldsymbol{f_1}(\boldsymbol{y_1}^{(k)}, \boldsymbol{z_1}^{(k)}) + A_{f_1}\cdot G_1 \cdot U^{(k)}_{Co,\bar{\boldsymbol{z}}_1} \\ \hline \boldsymbol{f_2}(\boldsymbol{y_2}^{(k)}, \boldsymbol{z_2}^{(k)}) + A_{f_2}\cdot G_2 \cdot U^{(k)}_{2,\bar{\boldsymbol{z}}_2} \\ (U^{(k)}_{2,\bar{\boldsymbol{z}}_2} - U^{(k)}_{1,\bar{\boldsymbol{z}}_2})/L \end{array}\right] \quad (3)$$

$$\boldsymbol{G} := \left[\begin{array}{l} \boldsymbol{g_1}(\boldsymbol{y_1}^{(k)}, \boldsymbol{z_1}^{(k)}) + A_{g_1}\cdot G_1 \cdot U^{(k)}_{Co,\bar{\boldsymbol{z}}_1} \\ (U^{(k)}_{B_1,\boldsymbol{y}_1} - U^{(k)}_{Co,\bar{\boldsymbol{z}}_1})\cdot G_1 + I^{(k-1)}_{Co,\bar{\boldsymbol{z}}_1}(t) \\ \hline \boldsymbol{g_2}(\boldsymbol{y_2}^{(k)}, \boldsymbol{z_2}^{(k)}) + A_{g_2}\cdot G_2 \cdot U^{(k)}_{2,\bar{\boldsymbol{z}}_2} \\ I^{(k)}_{Co,\bar{\boldsymbol{z}}_2} + I^{(k)}_{L,\bar{\boldsymbol{y}}_2} \\ (U^{(k)}_{2,\bar{\boldsymbol{z}}_2} - U^{(k)}_{B_2,\boldsymbol{y}_2})\cdot G_2 - I^{(k)}_{L,\bar{\boldsymbol{y}}_2} \\ U^{(k)}_{1,\bar{\boldsymbol{z}}_2} + U^{(k)}_{Co,\bar{\boldsymbol{z}}_2}(t) \end{array}\right] \quad (4)$$

where the incidence matrices $\boldsymbol{A}_{f\star}, \boldsymbol{A}_{g\star}$ stamp the currents $G_1 U_{Co,\bar{\boldsymbol{z}}_1}$, $G_2 U_{2,\bar{\boldsymbol{z}}_2}$ into the respective branch equation.

Using LR-coupling for system (2), one ends up with the (extended) recursion estimate with vectors

$$\left[\delta^{(k)}_{\boldsymbol{y}}, \delta^{(k)}_{\boldsymbol{z}}, \delta^{(k)}_{\star\bar{\boldsymbol{z}}_1}, \delta^{(k)}_{\star\bar{\boldsymbol{z}}_2}\right]^T \le \boldsymbol{K_e}\cdot\left[\delta^{(k-1)}_{\boldsymbol{y}}, \delta^{(k-1)}_{\boldsymbol{z}}, \delta^{(k-1)}_{\star\bar{\boldsymbol{z}}_1}, \delta^{(k-1)}_{\star\bar{\boldsymbol{z}}_2}\right]^T$$

$\delta^{(\cdot)}_{\boldsymbol{y}} = (\delta^{(\cdot)}_{\boldsymbol{y_1}}, \delta^{(\cdot)}_{\tilde{\boldsymbol{y}}_2})^T$, $\delta^{(\cdot)}_{\boldsymbol{z}} = (\delta^{(\cdot)}_{\boldsymbol{z_1}}, \delta^{(\cdot)}_{\boldsymbol{z_2}})^T$, $\delta^{(\cdot)}_{\star\bar{\boldsymbol{z}}_1} = \delta {U_{Co,\bar{\boldsymbol{z}}_1}}^{(\cdot)}$, $\delta^{(\cdot)}_{\star\bar{\boldsymbol{z}}_2} = (\delta {U_{1,\bar{\boldsymbol{z}}_2}}^{(\cdot)}, \delta {U_{2,\bar{\boldsymbol{z}}_2}}^{(\cdot)}, \delta {I_{Co,\bar{\boldsymbol{z}}_2}}^{(\cdot)})^T$ and (extended) recursion matrix $\boldsymbol{K}_e$. Convergence results are deduced by inspecting the eigenvalues of K_e. For the LR-coupling (Fig. 1) holds $\rho(K_e) = C_{I_{Co}}H$, where NW1 and NW2 are arbitrary (both of index1).

Proof. Basically we extend the proof from [2] by taking additional terms of the LR-coupling into account. For the algebraic unknowns of NW1, with $\boldsymbol{z_1} = \Phi_1(\boldsymbol{y_1})$, the estimation holds

$$|\Delta^{(k)}_{\boldsymbol{z_1}}| \le L_\Phi |\Delta^{(k)}_{\boldsymbol{y_1}}|, \quad (5)$$

where L_Φ is the maximum of the Lipschitz constants of ϕ_i. For the ODE-part, Lipschitz continuity yields:

$$|\Delta^{(k)}_{\boldsymbol{y_1}}| \le |\Delta^{(k-1)}_{\boldsymbol{y_1}}(t_n)| + \int_{T_n}^{T_{n+1}} L_f(|\Delta^{(k)}_{\boldsymbol{y_1}}| + |\Delta^{(k)}_{\boldsymbol{z_1}}|) + G_1\cdot|\Delta U^{(k)}_{Co,\bar{\boldsymbol{z}}_1}|\mathrm{dt}, \quad (6)$$

with Lipschitz constant L_f. Insert (5) into (6) and with algebraic constraint for $U^{(k)}_{Co,\bar{\boldsymbol{z}}_1}$ we obtain

$$\delta^{(k)}_{\boldsymbol{y_1}} \le \frac{1}{1-C_0H-G_1H}(|\Delta^{(k-1)}_{\boldsymbol{y_1}}(t_n)| + H\cdot\delta I^{(k-1)}_{Co,\bar{\boldsymbol{z}}_1}), \quad (7)$$

where $C_0 := L_f(1+L_\phi)$. Then inserting (7) into (5) and solving for $\delta^{(k)}_{\boldsymbol{z_1}}$ yields:

$$\delta^{(k)}_{\boldsymbol{z_1}} \le \frac{L_\Phi}{1-C_0H-G_1H}(|\Delta^{(k-1)}_{\boldsymbol{y_1}}(t_n)| + H\cdot\delta I^{(k-1)}_{Co,\bar{\boldsymbol{z}}_1}). \quad (8)$$

Similarly, using the same technique for subsystem 2, the corresponding estimate for $\delta I^{(k)}_{Co,\bar{\boldsymbol{z}}_2}$ reads:

$$\delta I^{(k)}_{Co,\bar{\boldsymbol{z}}_2} \le c\cdot|\Delta^{(k-1)}_{\tilde{\boldsymbol{y}}_2}(t_n)| + CH\cdot|\Delta^{(k-1)}_{\boldsymbol{y_1}}(t_n)| + C_{I_{Co}}H\cdot\delta I^{(k-1)}_{Co,\bar{\boldsymbol{z}}_1}, \quad (9)$$

with constants $c := 1/\left(1 - C_0H + \frac{L_f+G_2}{G_2}H + (L_f+G_2)H\right)$ $C := c\cdot L_f/(1-C_0H-G_1H)$ and $C_{I_{Co}} := c\cdot(\frac{L_f}{G_1}+CH)$. Because of $C_{I_{Co}}H$ is located on the diagonal of K_e, it determines the spectral radius of K_e. This conclude the proof. □

Thus LR-coupling provides convergence with rate $\mathcal{O}(H)$ for window size $H < H_{\max}$, while $C_{I_{Co}}$ is an indicator for the strength of coupling, having impact to the speed of contraction.

V. Test Circuit: Transformer

A transformer typically used in low frequency applications, connected by a wire to a voltage source serves as our test circuit for co-simulation, see Fig. 2.

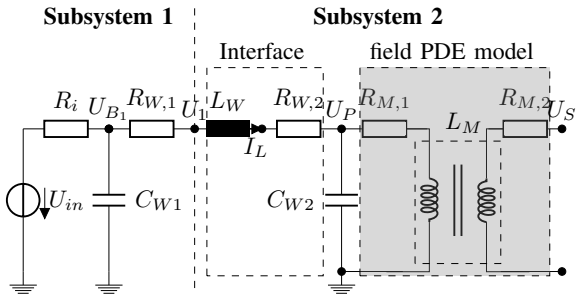

Fig. 2. Field/circuit coupling using LR-interface. Settings: $R_{W,1} = R_{W,2} =$ 1kΩ, $C_{W1} = C_{W2} =$ 1nF, $L_W =$ 1nH, $R_i = 10\Omega$ and supply voltage $U_{\text{in}}(t) = 170\text{V} \cdot \cos(\omega t)$ with $\omega = 2\pi \cdot 60$ Hz.

A. Technical Details

The resistances of the coil windings are simply extracted from the software package *Finite Element Method Magnetics* (FEMM), see [8], with $R_{M,1} = 0.449\ \Omega$ and $R_{M,2} = 0.062\ \Omega$. This transformer has 260 turns on the primary and 90 turns on the secondary side without load, dampens the secondary voltage U_{S} to a third of its primary voltage U_{P}. The coupling of the field and circuit part was realized in *FIDES*, see [9]. The transformer is modeled in 2D using spatial discretizations from FEMM, while the pure circuit part is setup via MNA. Applying finite element method the problem can be traced back to a common DAE-DAE coupling, see [5].

Still the data transfer is managed by time-dependent sources and the splitting scheme (3), (4) can be applied.

B. Convergence Analysis

Splitting at the EM-device boundaries (classical approach) and starting the iteration with the computation of the MQS device, Gauß-Seidel-type dynamic iteration of the field and circuit subproblems is unconditionally stable and convergent with convergence rate $\mathcal{O}(H)$, see [5]. This follows from the resulting coupling structure. Furthermore when co-simulation is started with the computation of the circuit, the old iterate of the MQS device, i.e., the primary current, enters differential equation. Thus no algebraic constraint depends on old algebraic iterate (simple coupling). Hence, in particular for the circuit in Fig. 2, general convergence is guaranteed independently from its computational order.

On the other hand, LR-coupling do not provides "simple coupling", because for both computational order, an algebraic constraints depends on old algebraic iterate. However convergence is guaranteed by a structural analysis, see Sec. 4.

VI. Numerical Simulations

To prove the concept, for any time integration (strong or weak coupled problem) the implicit Euler method was used with various step sizes. The time integrator steps sizes are chosen in such a way that the total points are sufficient to render the dynamics of the model. That is, that the time integration inaccuracies can be neglected.

A. Maximal Window Sizes and Waveform Progression

For both approaches (cutting at EM-device boundaries and LR-coupling), we investigate the maximum window size for convergence. For time-integration of each subproblem the implicit Euler method with Newton tolerance of 10^{-6} was applied. Fig. 3 shows the waveform progression of the primary voltage in the first time window $[0, H]$ for iteration steps $k = 1, \ldots, 10$. We find that LR-coupling enables time window

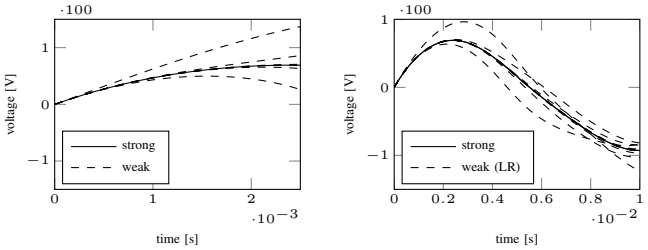

Fig. 3. Waveforms of primary voltage on $[0, H]$ for iterations $k = 1, \ldots, 10$. (left) classical approach, $H = 2.5$ ms. (right) LR-coupling, $H = 10$ ms.

sizes up to $H = 10$ s (maximal tested window; Fig. 3 (right) shows only a cutout), while for the classical approach the maximum possible window size for convergence is $H = 2.5$ ms, see Fig. 3 (left). However, the use of very large window sizes usually increases the number of iterations to reach a certain tolerance.

B. Convergence Rate

To verify the rate of convergence, we inspect the lumped error in the primary and secondary voltages as well as in the primary current of the transformer, see Fig. 2. We employ constant extrapolation for the coupling variables, which is the most common guess to start up co-simulation. Starting with zeros as initial setting for the initial value problem, we first solve the model (strong and weak coupled) up to $t_0 = 0.001$ s for consistency. Then, our co-simulation is only performed on the first time window $[t_0, t_0 + H]$ with consistent initial values. Thus, no error transport between several time windows occurs, which ensures to measure the pure splitting error due to stopping co-simulation after $k = 1$ iteration.

For LR-coupling as well as for the standard field/circuit decoupling we use the same step size for the applied time integrator, hence no interpolation technique is required for error measurement. The errors are given with respect to the corresponding reference solution.

Fig. 4 shows the error obtained for various time window sizes concerning the primary U_{P} and secondary voltages U_{S} of the transformer. Thus, for both approaches the gain of accuracy per iteration in U_{P} and U_{S} is $\mathcal{O}(H)$. This fits to the preceding theory for LR-coupling.

However, a higher convergence rate of $\mathcal{O}(H^2)$ is obtained concerning the primary current of the transformer, see Fig. 5 (solid line). This behavior can explained as follow: The old iterate which enters subsystem 1, i.e., the current $I_{Co}^{(k-1)}$, is directly linked by the induction current $I_L^{(k)}$ using Kirchhoff's current law $0 = I_{Co}^{(k-1)} + I_L^{(k)}$. Recall that $I_L^{(k)}$ is differential, thus it is obtained by time integration. With C_{W2} small

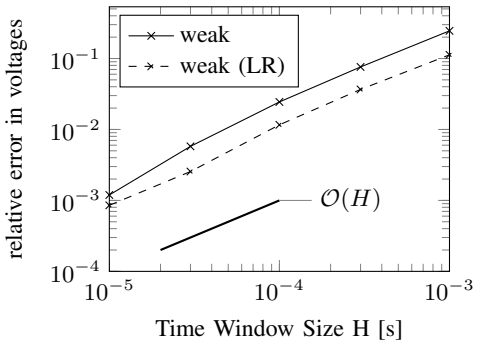

Fig. 4. Convergence plot of the field/circuit co-simulation concerning the primary and secondary voltages for different time window sizes H with one iteration per time window after $t_0 = 0.001$ ms with and without LR-coupling.

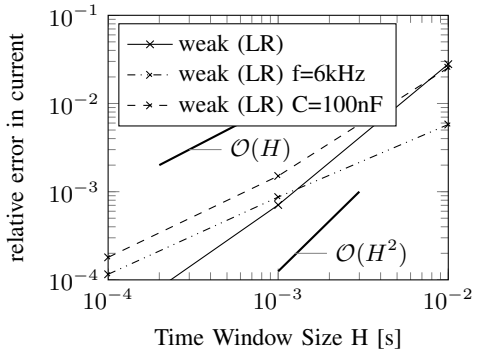

Fig. 5. Convergence plot concerning the primary current for different time window sizes H with one iteration per time window after $t_0 = 0.001$ ms for an increased frequency and capacitance.

enough (in our case $C_{W2} = 1$nF) the capacity connected to ground can be neglected, thus there is only a negligible current flowing through the capacitor against ground. Again, Kirchhoff's current law for the primary current yields a direct link to the induction current I_{L_W}, i.e., $0 = I_p + I_{L_W}$ holds for slow alternating node potential U_P and C_{W2} small enough. Therefore, waveform progression of the primary current is enhanced in the time integrator. The lumped error in all unknowns will remain unaffected. Thus, LR-coupling provides overall $\mathcal{O}(H)$, while the error behavior of the primary current benefits from its surrounding circuit structure.

To confirm this effect, we repeat co-simulation with an increased capacitance of $C_{W2} = 100$ nF as well as for an increased frequence of $f_\mathrm{in} = 6$ kHz. In this case the current through the capacitance becomes more important. Notice that this current is governed by its node potential U_P which offers convergence rate $\mathcal{O}(H)$, see Fig. 5. Thus the primary current of the transformer cannot longer benefit from its surroundings.

Fig. 6 compares the contraction behavior of LR and standard field/circuit decoupling on $[0,\ 0.02]$ s (about one cycle). We used the largest possible window size of the classical approach: $H = 2.5$ ms.

In addition, LR-coupling enables for a faster waveform propagation. The speed of convergence depends on different leading coefficients, e.g. $C_{\mathrm{I_{Co}}}$, reflecting the strength of coupling. Thus both schemes converge before they are bounded by the time integrator accuracy of about 10^{-4}.

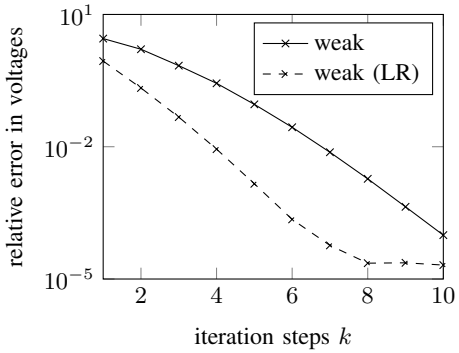

Fig. 6. (left) Error in primary and secondary voltages in dependence of the iteration k in $[0, 0.02]$ s, using window size $H = 2.5$ ms for both approaches.

VII. CONCLUSIONS

We proposed a new approach for coupling (LR-coupling), where convergence is guaranteed for each choice of electrical networks, i.e. circuit or EM device, and for each computational order. We showed that LR-coupling provides a guaranteed convergence rate of $\mathcal{O}(H)$, which has been verified numerically. Regarding the maximum possible window size, we showed that cutting at the EM device boundary does not always works best and showed that using LR-coupling enables to enlarge the window sizes multiple times. Additionally, our coupling structure yields better properties regarding the speed of contraction. Therefore, for an efficient scheme the interplay between window size and number of iterations needs to be carefully investigated.

Also the general design of coupling interfaces with best co-simulation properties in the field/circuit context need further attention. In the future, we also aim at including uncertainty into the convergence analysis.

ACKNOWLEDGMENT

This work is supported by the German Federal Ministry of Education and Research (BMBF) in the research projects SIMUROM, (05M13PXB) and KoSMos, (05M13PXA).

REFERENCES

[1] Arnold, M., Günther, M.: Preconditioned Dynamic Iteration for Coupled Differential-Algebraic Systems. In: BIT, vol. 41, pp. 1–25 (2001)
[2] Bartel, A., Brunk, M., Günther, M. and Schöps, S.: Dynamic Iteration for Coupled Problems of Electric Circuits and Distributed Devices. SIAM J. Sci. Comput., vol. 35, No. 2, pp. B315–B335 (2013).
[3] Burrage, K.: Parallel and Sequential Methods for Ordinary Differential Equations. Oxford, U.K.: Oxford Univ. Press, 1995.
[4] Bartel, A., Brunk, M., Schöps, S.: On the convergence rate of dynamic iteration for coupled problems with multiple subsystems. J. Comput. Appl. Math., vol. 262, pp. 14–24 (2014)
[5] Schöps, S., De Gersem, H., Bartel, A.: A Cosimulation Framework for Multirate Time Integration of Field/Circuit Coupled Problems. In: IEEE Trans. Magn., vol. 46, No. 8 (2010)
[6] De Gersem, H., Weiland, T.: Field-circuit coupling for time-harmonic models discretized by the finite integration technique In: IEEE Trans. Magn., vol. 40, No. 2, pp. 1334-1337 (2004)
[7] Lange, E., Henrotte, F., Hameyer, K.: A circuit coupling methode based on a temporary linearization of the energy balance of the finite element model In: IEEE Trans. Magn., vol. 44, No. 6, pp. 838-841 (2008)
[8] Meeker, D.: Finite Element Method Magnetics - User's Manual: http://www.femm.info/Archives/doc/manual42.pdf
[9] Schöps, S.: Field Device Simulator: http://www.schoeps.org/home